Journal of Southeast University (English Edition) Vol. 40, No. 2, pp. 111 - 119 June 2024 ISSN 1003—7985

Dynamic testing and parameter identification for tuned viscous mass dampers

Ji Xiaodong Cheng Yuhao Jia Ruofan Yu Yue

(Key Laboratory of Civil Engineering Safety and Durability of Ministry of Education, Tsinghua University, Beijing 100084, China)

Abstract: A novel type of tuned viscous mass damper (TVMD) device incorporating eddy current damping and metal springs as its damping and spring elements, respectively, was developed. First, dynamic tests of the TVMDs were conducted to investigate their dynamic characteristics. Subsequently, four methods were proposed to identify the TVMD parameters from the test data: the peak point fitting method, hysteretic curve fitting method, time-history fitting method, and transfer function fitting method. The dynamic test results indicate that the TVMD exhibits the inertial mass amplification and damping enhancement effects. The spring and inerter elements demonstrate ideal linear behavior, while the damping element exhibits nonlinearity, primarily owing to the nature of eddy current damping and inherent friction in the TVMD device. The parameter identification results indicate that all four methods can reasonably determine the TVMD parameters. The transfer function fitting method can provide an equivalent damping coefficient useful for tuning design, while the other three methods can identify parameters of nonlinear damping models. The hysteretic curve fitting and time-history fitting methods exhibit improved accuracy in parameter identification, while the peak point fitting and transfer function fitting methods exhibit higher computational efficiency.

Key words: tuned viscous mass damper (TVMD); dynamic test; parameter identification; damping nonlinearity; vibration control

DOI: 10.3969/j.issn.1003 - 7985.2024.02.001

In civil engineering, structural vibration control is a pivotal technique for enhancing the performance of structures subjected to dynamic loads such as seismic motions and wind loads. To date, various types of dynamic vibration absorbers have been proposed[1-7]. Among these, the tuned viscous mass damper (TVMD), a novel type of inerter-based vibration absorber, is promising for application in buildings and civil infrastructures[5]. The TVMD is characterized by the inertial mass amplification mechanism and the damping enhancement effect[8]. The TVMDs installed in a structure serve to tune a target structural mode and provide supplementary damping for the lower-order modes[9], thereby demonstrating their ability to control the seismic responses of both inter-story drifts and floor accelerations[10-11]. The superior performance of the TVMD for controlling dynamic responses of various structural systems, such as the frame structure[12], coupled wall structure[11,13], and core wall structure[14], has been demonstrated. TVMDs have been employed in real-world buildings in Japan, including a telecommunication building (a 15-story frame structure in Sendai)[12], Akasaka Intercity (a 37-story building in Tokyo)[15], and the Shinjuku Sumitomo Building (a retrofitted 54-story building in Tokyo)[16].

The TVMD consists of an inerter element and a dashpot element arranged in parallel, forming a viscous mass damper (VMD), which is then linked to a spring element in series. The inerter element is a mechanical element with a parameter known as "inertance," which can be expressed in units of mass[17]. However, different from the general mass element, the inertial force generated by the inerter element is proportional to the relative acceleration between its two terminals. Over the past twenty years since the inerter was proposed, various types of approaches have been developed to realize the inerter element[5,18-19], among which the ball screw system has proved to be promising[5]. This system utilizes a motion conversion mechanism that converts linear motion into rapid rotational motion to generate substantial inertial force with a small physical mass. Through this mechanism, the damping element, which is in parallel to the inerter element, can generate an extremely amplified damping force. By connecting the spring element with the VMD in series, the TVMD has a natural vibration frequency, enabling it to tune a selected mode of the structure, similar to a tuned mass damper[4,20-21].

Various methods have been proposed for the optimal tuning design of TVMDs[5,22]. However, achieving successful TVMD tuning control requires the actual parameter values of TVMDs to closely match the design values. Unfortunately, there is a lack of standardized methods for

Received 2024-02-06, **Revised** 2024-04-10.

Biography: Ji Xiaodong (1979—), male, doctor, associate professor, jixd@mail.tsinghua.edu.cn.

Foundation items: The National Natural Science Foundation of China (No. 52078277), Foundation of the Institute for Guoqiang of Tsinghua University (No. 2020GQC0003).

Citation: Ji Xiaodong, Cheng Yuhao, Jia Ruofan, et al. Dynamic testing and parameter identification for tuned viscous mass dampers[J]. Journal of Southeast University (English Edition), 2024, 40(2): 111 - 119. DOI: 10.3969/j.issn.1003 - 7985.2024.02.001.

accurately identifying TVMD parameters. To fill this gap, this paper aims to develop methods for accurately extracting the parameter values of TVMD devices from experimental test data. The study introduces two novel contributions: 1) the development of a novel TVMD device using eddy current damping and metal springs, and 2) the proposal of four methods for TVMD parameter identification.

1 Dynamic Tests of TVMDs

1.1 TVMD devices

Fig. 1 depicts the TVMD mechanical model, which is composed of a spring element connected to the VMD in series. In this study, three TVMDs labeled as T-1, T-2, and T-3 were manufactured. The three devices were nearly identical, except that T-3 had slightly larger damping than the other two. The reason for testing three devices was to validate the performance stability of this novel type of device. The configuration of the TVMD device is depicted in Fig. 2. The spring element (from point A to point C) consisted of nine rods (one central main rod and eight secondary rods positioned on the periphery) and sixteen metal compression springs (eight on the left and eight on the right, separated by a middle panel). The main rod transmitted axial loads and torque generated by the VMD element, being fixed to the middle panel to ensure identical displacements of points D and B. The relative motion of points D and B with respect to the right endpoint O represented the displacement of the VMD element, denoted as u_d. The secondary rods served to transfer load and prevent the buckling of the metal springs under compression. Due to the constraints imposed by these rods, points A and C, representing the two end plates of the spring element, exhibited identical movement. The movement of points A and C relative to point O represented the displacement of the TVMD, denoted as u_t. Additionally, as illustrated in Fig. 2, linear guide sticks were utilized to enable the spring element and VMD element to deform along the axial axes of the TVMD consistently. When the middle panel shifted from its original position, the eight metal springs on one side (either the left or right side) were compressed, while the springs on the other side remained free. Therefore, the stiffness of the spring element was calculated as eight times the stiffness of a single metal compression spring. An axial compression test conducted on a single metal spring indicated a stiffness of 232.3 kN/m. Therefore, the spring element had a nominal stiffness of 1 858.4 kN/m.

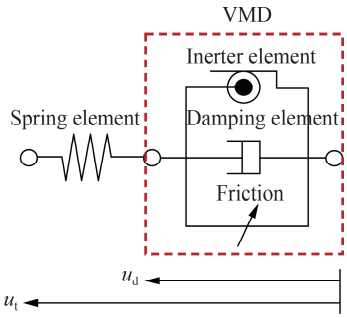

Fig. 1 TVMD mechanical model

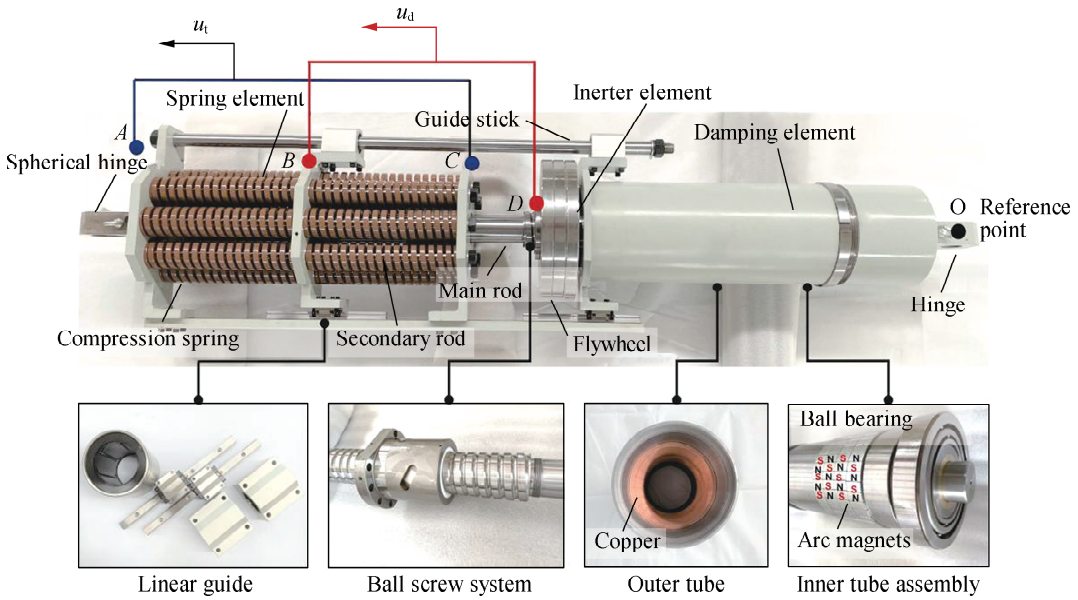

Fig. 2 TVMD configuration

The VMD was formed by a ball screw system, while the inerter element consisted of flywheels based on the ball screw system. The inertance of the TVMD could be altered by adjusting the moment of inertia of the flywheels attached to the nut of the ball screw. The physical mass of the inerter element was 73.7 kg. The damping element comprised two tubes (an outer tube and an inner tube) and permanent arc magnets. Eddy current damping can be generated through the relative motion of a conductor in a constant magnetic field produced by permanent magnets.

The inner tube was fixed to the nut of a ball screw and rotated when driven by the ball screw system. The iron inner tube acted as a back iron, enhancing the intensity of the magnetic field outside the inner tube and further amplifying the impulsive forces. To serve as the conductor, a 10 mm thick copper tube was attached to the inner surface of the carbon steel outer tube. The magnetic field between the inner tube and outer tube was generated by radial-magnetized permanent arc magnets, with adjacent magnets having opposite magnetic poles. A total of 136 pieces of permanent arc magnets were used, each with a projection area of 30 mm × 15 mm and a thickness of 3 mm. The air gap between the outer surface of the arc magnets and the inner surface of the conductor was 2 mm. The permanent arc magnets of T-3 were different from those of T-1 and T-2, with the former resulting in a larger magnetic field than the latter. Apart from this distinction, the three manufactured TVMDs were identical.

1.2 Test setup, instrumentation, and loading protocols

The specimens were loaded by a uniaxial dynamic loading facility, as depicted in Fig. 3. Displacement transducers LVDT-1 and LVDT-2 were used to measure the displacement of the VMD element u_d and spring element u_s, respectively. The axial force was measured by the load cell located at the terminal of the TVMD device.

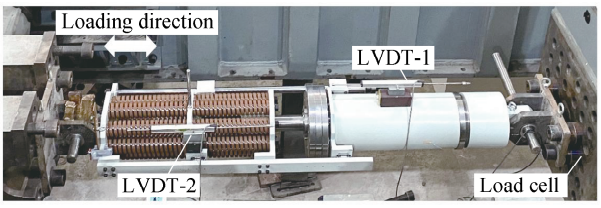

Fig. 3 Dynamic test setup

The experimental program involved two phases. Initially, quasi-static cyclic loads were applied to determine the sliding friction force of the ball screw system, with an amplitude of ±60 mm and a loading velocity of 6 mm/s. Subsequently, dynamic loads were applied to examine the dynamic properties and responses of the TVMDs, consisting of a series of displacement-controlled sinusoidal loads. The loading amplitudes were ±20 and ±27 mm (with an additional ±23.5 mm test for T-2), and the frequency f_0 of the sinusoidal loads varied from 0.1 to 1.4 Hz, with an increment of 0.1 Hz. Five cycles of loads were repeated at each loading frequency until the TVMD reached a steady-state response. Furthermore, it is important to note that an increased number of loading cycles (e.g., 7 to 10) were applied at the loading frequencies that were near the natural frequency of the TVMDs, as they required a longer duration to reach their steady-state responses.

1.3 Experimental results

1.3.1 Quasi-static loading test

To ensure adequate stiffness of the high-performance ball screw systems, the balls in the ball nut were preloaded during the production process. The precompression load resulted in inherent friction in the ball screw systems. Fig. 4 depicts the hysteretic responses of the VMD under quasi-static loading. The VMD element exhibited "stop-to-go" behavior, indicating that the dry friction was greater than the sliding friction. The sliding friction was determined as the lower boundary of the axial force values (i.e., 5 kN), as displayed in Fig. 4.

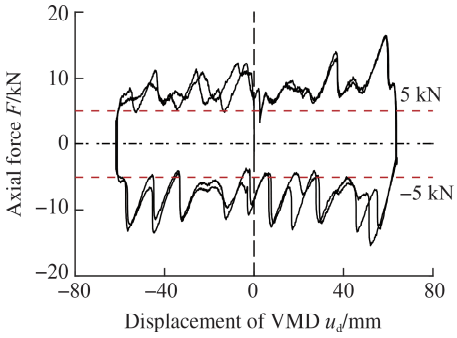

Fig. 4 Hysteretic curve of the VMD under quasi-static loading

1.3.2 Dynamic loading test

Fig. 5 displays the displacement response history of T-1 at loading frequencies of 0.4, 0.8 (approximately the natural frequency of TVMD), and 1.2 Hz in the 27 mm-magnitude dynamic tests. In Fig. 5, γ denotes the ratio of the excitation frequency to the TVMD natural frequency. As indicated, the spring displacement u_s demonstrated phase advance compared with the TVMD displacement u_t, while the VMD displacement u_d exhibited phase lag compared with u_t. When the loading frequency f_0 was close to the TVMD natural frequency (see Fig. 5(a)), both u_s and u_d were significantly amplified compared with u_t, and the spring element and the VMD element had a phase angle of approximately 180°. Fig. 5(b) depicts the transfer functions from the TVMD total displacement u_t to the displacement of the VMD element u_d and the spring element u_s. When the loading frequency was substantially lower than the natural frequency of TVMD($\gamma \ll 1$), the VMD response dominated the total displacement of the TVMD (see Fig. 5(c)). In contrast, the displacement of the spring element was extremely limited because the stiffness of the spring was much greater than the equivalent dynamic stiffness of the VMD. This resulted in cyclic responses of the VMD with a large magnitude, thus providing energy dissipation and damping supplementation in lower-frequency vibration. Conversely, when the loading frequency was substantially higher than the natural frequency of the TVMD ($\gamma \gg 1$), the displacement of the spring far exceeded the displacement of the VMD (see

Fig. 5(d)). Here, the cyclic response of the VMD exhibited a relatively low magnitude, offering limited damping during higher-frequency vibration. As the loading frequency approached the natural frequency of the TVMD ($\gamma \approx 1$), resonance occurred, resulting in opposite deformations of the spring element and the VMD element (see Fig. 5(a)). The motion of the VMD experienced significant amplification, leading to substantial supplementary damping of the vibration. This finding aligns with Ref. [11], which demonstrated that under TVMD natural frequency loading, the spring element and the VMD element deformed in opposite directions. This phenomenon contributed to the damping amplification effect of the TVMD, as the increased displacement of the VMD enhanced energy dissipation.

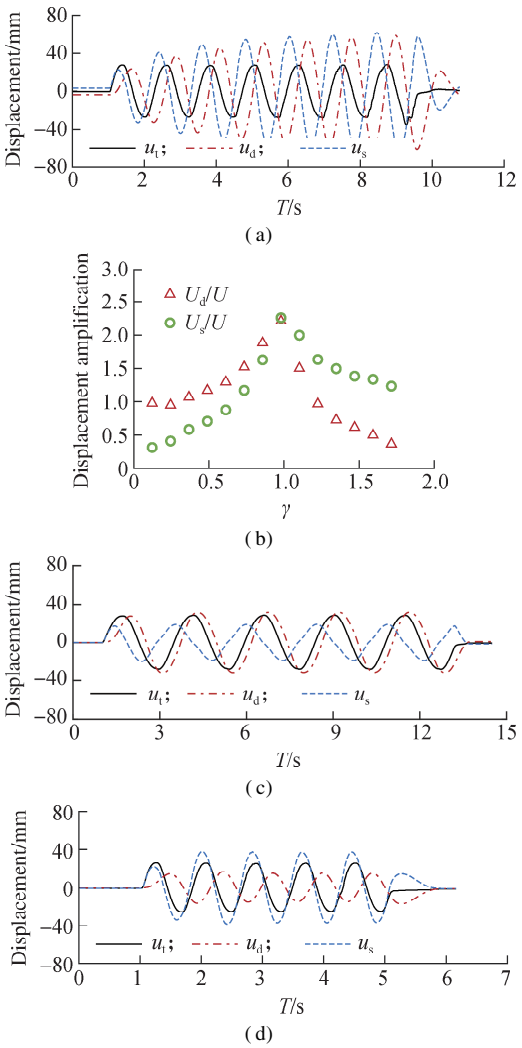

Fig. 5 Displacement response of T-1. (a) Response history at f_0 = 0.8 Hz; (b) Transfer function; (c) Response history at f_0 = 0.4 Hz; (d) Response history at f_0 = 1.2 Hz

Fig. 6 depicts the hysteretic curves of T-1 at loading frequencies ranging from 0.1 to 1.4 Hz in 27 mm-magnitude tests. The thick dashed lines represent the hysteretic response at a loading frequency of 0.8 Hz. At 0.8 Hz loading, the TVMD's hysteretic curve was fully developed (see Fig. 6(a)), indicating significantly enhanced energy dissipation capacity. The spring element exhibited linear behavior (see Fig. 6(b)), while the VMD element displayed a combination of negative stiffness and viscous damping (see Fig. 6(c)). The former was caused by the inerter element, and the latter was due to the eddy current damping. Similar test results were observed for T-2 and T-3.

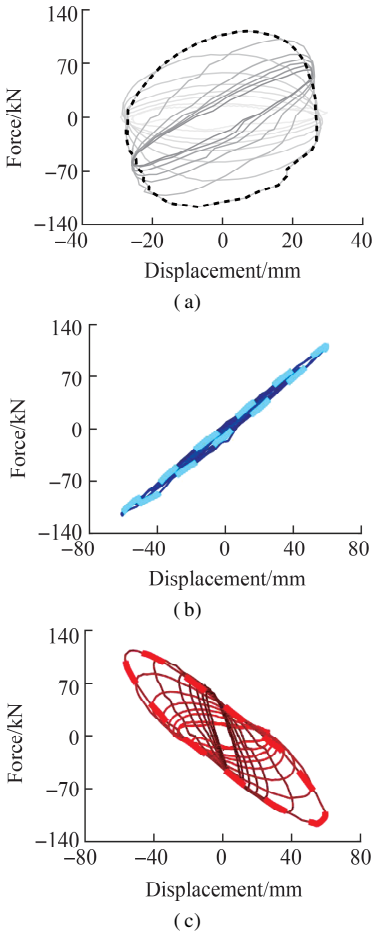

Fig. 6 Hysteretic curve of T-1. (a) TVMD; (b) Spring element; (c) VMD element

2 Parameter Identification of TVMD

2.1 Parameter identification of the spring element

Owing to the linear behavior of the spring element, its stiffness was determined through linear fitting of $F = k_b u_s$ where F and u_s represent the axial force and displacement of the spring element, respectively. Table 1 lists the linear fitting results of spring stiffness for each TVMD specimen based on data from all dynamic loading tests. The stiffness values were nearly identical for all three TVMDs and closely matched the nominal stiffness value of 1 858.4 kN/m obtained from axial compression tests on the springs.

Table 1 Estimated stiffness of the spring element

Specimen No.	T-1	T-2	T-3
Stiffness k_b/(kN · m^{-1})	1 878.5	1 892.7	1 873.6

2.2 Parameter calibration of VMD element

As shown in Fig. 1, three components contributed to the total force of the VMD: the inertial force, eddy current damping force, and sliding friction force. Four methods were proposed to identify the parameters of the VMD element: 1) the peak point fitting method, 2) the hysteretic curve fitting method, 3) the time-history response fitting method, and 4) the transfer function fitting method.

2.2.1 Peak point fitting method

In this method, the inertial mass and damping parameters were determined by fitting the force-peak-acceleration data and the force-peak-velocity data of the VMD, respectively. These relationships were derived from the displacement response history of the VMD element when the system reached a steady state. Specifically, when the displacement of the VMD $u_d = 0$, the acceleration $\ddot{u}_d = 0$ and the velocity $\dot{u}_d$ reached their peak values, indicating that the VMD force was caused by the dashpot element and friction. Similarly, when u_d reached its peak value, $\dot{u}_d = 0$ and $\ddot{u}_d$ also reached its peak value, indicating that the VMD force was generated by the inerter element and friction.

The force-displacement response data from the last cycle of the steady-state response under each loading frequency were utilized to derive the force-peak-acceleration data and force-peak-velocity data. For both positive and negative loading in the final loading cycle, the test data at the peak displacement U of VMD were selected as the peak points, and the corresponding force was designated as the VMD force at the peak displacement. Similar to the steady-state response of sinusoidal vibration, peak acceleration coincided with peak displacement, with a magnitude of $A = \omega^2 U$, where ω represents the loading frequency. Furthermore, when a sufficient number of data points were selected, the number of points with positive velocity direction and those with negative velocity direction were nearly identical, minimizing the influence of constant friction f_0 on the fitting results. Fig. 7 illustrates the fitting results for the force-peak-acceleration relationship, demonstrating an ideal linear characteristic of the inerter element. The fitting results are detailed in Table 2. The apparent mass of the inerter element, with an average value of 72.3 t, was approximately 1 000 times its physical mass of 73.7 kg. This represents the inertial mass amplification effect of the TVMD.

Table 2 Values of inerter mass estimated through the direct fitting method

Specimen No.	T-1	T-2	T-3
Inertial mass m_r/t	71.5	72.6	72.7

The peak value point was selected from the test data at displacement $u_d = 0$. Similar to the calculation of peak

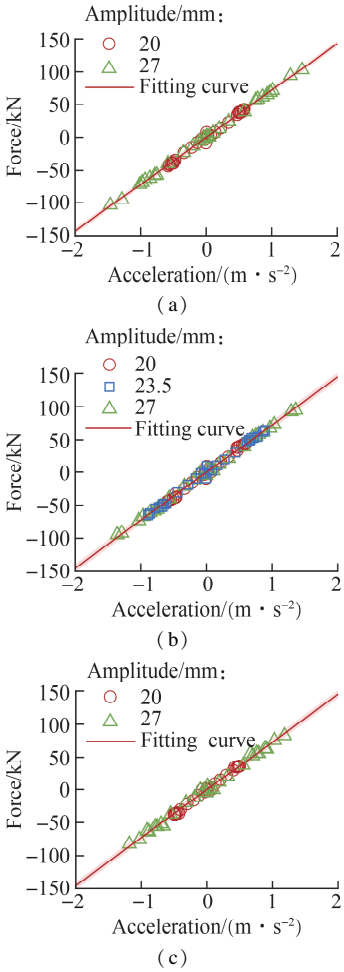

Fig. 7 Curve fitting for the inerter element estimated through the direct fitting method. (a) T-1; (b) T-2; (c) T-3

acceleration, the peak velocity V under sinusoidal loading was computed as $V = \omega U$. This study considered three damping models: 1) the equivalent linear damping model, commonly used in TVMD tuning design; 2) the exponential damping model, reflecting the nonlinearity of the dashpot element and often utilized in finite element analysis software; and 3) the Wouterse damping model[23], which accurately describes eddy current damping characteristics across a wide range of loading velocities, including damping force degradation at high-velocity loading. Wouterse[23] has revealed that when the velocity exceeds a critical value, the eddy current damping force will decrease. The aforementioned three damping models are formulated as

$$F_d = c_d v \tag{1}$$

$$F_d = \mathrm{sign}(v)\, c_{exp} v^{\alpha} \tag{2}$$

$$F_d = F_{max} \frac{2}{v/v_{cr} + v_{cr}/v} \tag{3}$$

where F_d and v denote the damping force and velocity, respectively; c_d and c_{exp} denote the damping coefficient of the equivalent linear model and exponential damping model, respectively; α denotes the equivalent damping exponent; v_{cr} and F_{max} denote the critical velocity and cor-

responding damping force, respectively.

The damping model parameters were identified by fitting the peak-velocity point data of all dynamic loading tests. During the fitting, the additional friction force f_0 was considered in the exponential damping model and the Wouterse damping model but not in the equivalent linear damping model. Fig. 8 displays the fitting curves of the damping models (the shaded area represents the region within two standard deviations of the error between the experimental force value and the fitting results). The identified parameters for these models are listed in Table 3. The linear damping model provided an equivalent representative of the eddy current damping in a region of velocity but could not consider the nonlinearity at high velocity and the friction effect. The small standard deviation values for the errors indicate that the exponential damping model and the Wouterse damping model reasonably captured the nonlinearity of the VMD element. Particularly, the fitted curve of the Wouterse damping model reflected the decrease in damping force at over-critical velocity.

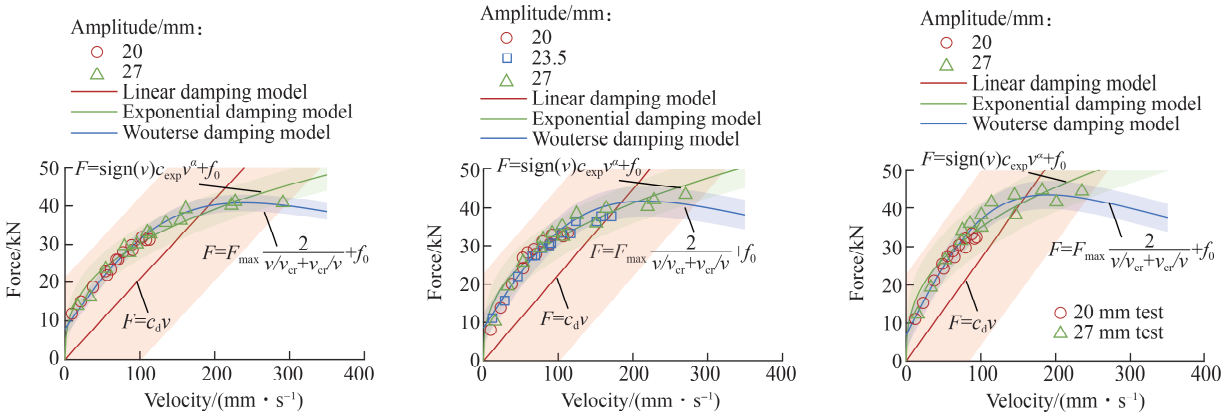

Fig. 8 Curve fitting for damping parameters estimated through the peak point fitting method. (a) T-1; (b) T-2; (c) T-3

Table 3 Values of damping parameters estimated through the peak point fitting method

Damping model	Parameters	T-1	T-2	T-3
Equivalent linear damping model	Equivalent damping coefficient c_d/(kN · s · m^{-1})	208.8	224.4	268.9
Exponential damping model	Exponential damping coefficient c_{exp}/(kN · s$^{\alpha}$ · m$^{-\alpha}$)	71.2	73.9	83.2
	Equivalent damping exponent α	0.37	0.36	0.38
	Constraint friction f_0/kN	0	0	0
Wouterse damping model	Critical damping force F_{max}/kN	32.8	33.2	36.6
	Critical velocity v_{cr}/(m · s^{-1})	0.24	0.22	0.19
	Constraint friction f_0/kN	8.0	8.5	6.8

2.2.2 Hysteretic curve fitting method

The force of the VMD element under sinusoidal loading was calculated by

$$F = m_r\ddot{u} + F_d(\dot{u}) = -\omega^2 m_r u + F_d(\dot{u}) \quad (4)$$

The velocity of the VMD $\dot{u}$ was obtained from the displacement time history using the interpolation method, and the acceleration was calculated according to the assumption $\ddot{u} = \omega^2 u$ for the sinusoidal steady-state response.

According to the steady-state hysteretic response data of 27 mm-magnitude dynamic tests at loading frequencies ranging from 0.1 to 1.4 Hz, the parameters of the aforementioned three damping models were identified through the least square method. The fitting results are presented in Fig. 9 and Table 4. Consistent with the observation from Fig. 8, the equivalent linear damping model overestimated the damping at high velocities (see Fig. 9(a)), resulting in a higher estimation of damping forces at zero-displacement regions. The fitting results of the other two damping models agreed well with the experimental data, as shown in Figs. 9(b) and (c).

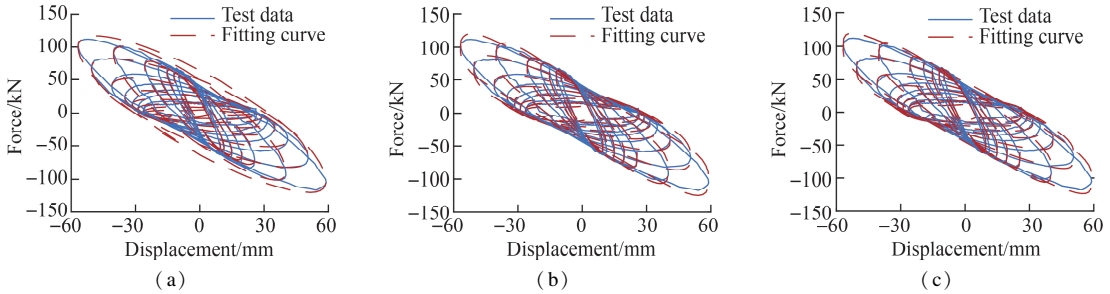

Fig. 9 Curve fitting for T-1 obtained through the hysteretic curve fitting method. (a) Equivalent linear damping model; (b) Exponential damping model; (c) Wouterse damping model

Table 4 Values of damping parameters estimated through the hysteretic curve fitting method

Damping model	Parameters	T-1	T-2	T-3
Equivalent linear damping model	Equivalent damping coefficient c_d/(kN · s · m^{-1})	217.4	225.2	273.2
Exponential damping model	Exponential damping coefficient c_{exp}/(kN · s$^{\alpha}$ · m$^{-\alpha}$)	88.4	87.8	106
	Equivalent damping exponent α	0.55	0.55	0.56
	Constraint friction f_0/kN	0.6	1.5	0.0
Wouterse damping model	Critical damping force F_{max}/kN	34.3	33.2	36.1
	Critical velocity v_{cr}/(m · s^{-1})	0.27	0.26	0.21
	Constraint friction f_0/kN	4.4	5.1	3.4

2.2.3 Time-history fitting method

To accurately calculate the velocity and acceleration response history of the VMD element, a finite element model of the VMD was developed in OpenSees. The inerter element was represented by an InertiaTruss element[13]. The dashpot element was modeled using a Truss element with Viscous material adopting an exponential damping model. Friction f_0 was simulated using a Viscous material with an equivalent damping exponent $\alpha = 0$. The time-history response of a VMD under a given load can be calculated from the nonlinear FE models in OpenSees. Optimization algorithms are utilized to determine the parameters of the nonlinear model by minimizing the difference between the FE-estimated responses and the test data. In this study, the genetic algorithm (GA) was chosen for nonlinear optimization due to its effective global search capability. As depicted in Fig. 10, the optimization process was conducted using a Matlab program, which interacted with the OpenSees program to estimate the nonlinear displacement history responses, compare them with the test data (U_T), and adjust the TVMD parameters accordingly. In this GA-based optimization, an initial population of 200 individuals was selected. The best-matching parameter values were determined after 3 000 rounds of iterations. The fitting results are listed in Table 5, and the fitting curve of T-1 is illustrated in Fig. 11.

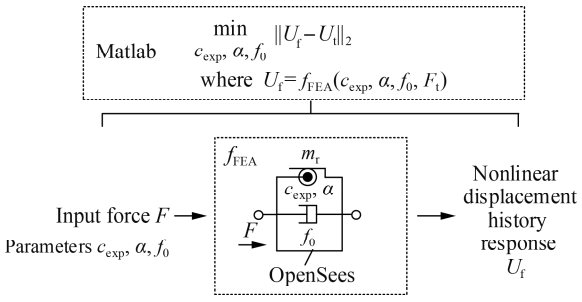

Fig. 10 Time-history fitting method

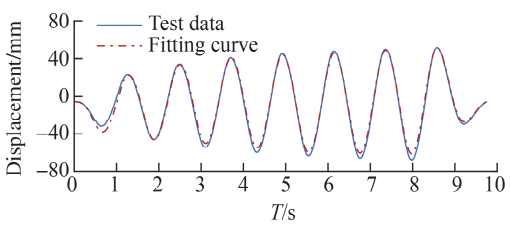

Fig. 11 Curve fitting for T-1 obtained through the time-history fitting method

Table 5 Values of inertial and damping parameters estimated through the time-history fitting method

Specimen No.	T-1	T-2	T-3
Inertial mass m_r/t	71.4	73.5	72.7
Exponential damping coefficient c_{exp}/(kN · s$^{\alpha}$ · m$^{-\alpha}$)	88.7	93.3	88.6
Equivalent damping exponent α	0.54	0.54	0.49
Constraint friction f_0/kN	2.1	1.6	1.0

Fig. 11 indicates that the time-history fitting method provided satisfactory estimation results that correlated well with the test data of the VMD element. The time-history fitting method utilized the complete time-domain response data rather than being limited to steady-state response data.

2.2.4 Transfer function fitting method

The transfer function of the TVMD can be derived from the equation of motion, considering the equivalent linear damping model. The transfer functions from TVMD displacement to spring displacement and VMD displacement[24] are presented as

$$\frac{U_s}{U} = \sqrt{\frac{\omega^4 m_r^2 + \omega^2 c_d^2}{(k_b - \omega^2 m_r)^2 + (c_d \omega)^2}} \tag{5}$$

$$\frac{U_d}{U} = \frac{k_b}{\sqrt{(k_b - \omega^2 m_r)^2 + (c_d \omega)^2}} \tag{6}$$

The equivalent linear damping coefficient could be determined by fitting Eq. (5) or (6) to the measured transfer function data, while the spring stiffness and inertial mass values from Tables 1 and 2 were used. Table 6 and Fig. 12 illustrate the fitting results and curves of the transfer function based on Eq. (6) alongside the 27 mm test results. The shaded area represents the region within two standard deviations of the error between the measured transfer function data and the fitting results (see Fig. 12). The addition of sliding friction (i.e., Coulomb damping) resulted in larger equivalent linear damping under small displacements. Consequently, the transfer function of the 20 mm-magnitude loading test was smaller than that of the 27 mm-magnitude loading test, as depicted in Fig. 12.

Table 6 Values of equivalent damping coefficient estimated through the transfer function fitting method

Specimen No.	T-1	T-2	T-3
Equivalent damping coefficient c_d/(kN · s · m^{-1})	209.6	219.4	255.4

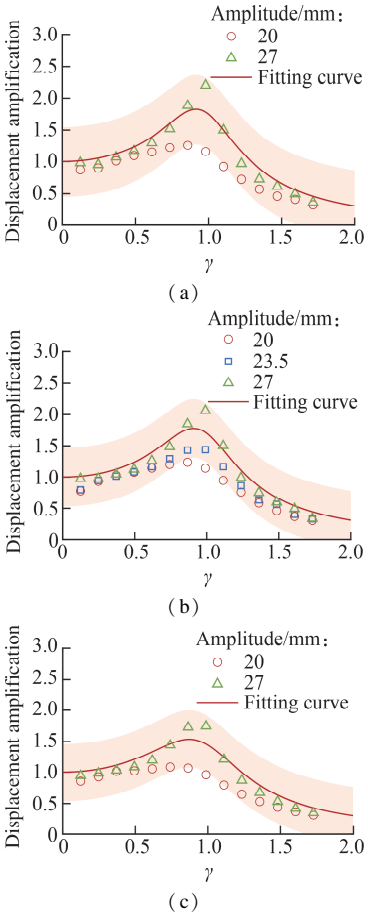

Fig. 12 Curve fitting for damping element obtained through the transfer function fitting method. (a) T-1; (b) T-2; (c) T-3

Additionally, the transfer function fitting method cannot account for the nonlinearity of the system.

2.3 Comparison and discussion

The transfer function fitting method offers a representative equivalent damping coefficient suitable for tuning design but cannot estimate parameters for nonlinear damping models. Conversely, the other three methods can identify parameters for nonlinear damping models. Among them, the time-history fitting method and hysteretic curve fitting method provide more precise estimations of TVMD parameters compared with the peak point fitting method, largely owing to their utilization of a larger volume of dynamic response data.

In terms of computational costs, the peak point fitting method demonstrates the most efficient performance, as it utilizes limited amounts of crucial test data. The transfer function method also has low computational costs, while the costs of the hysteretic curve fitting method and time-history fitting method are relatively high owing to their utilization of full response data.

3 Conclusions

1) A TVMD device incorporating metal springs and eddy current damping was developed. The test results indicate that the spring element and the inerter element exhibits ideal linear behavior, while the dashpot element displays a nonlinear force-velocity relationship, primarily attributed to the unique characteristics of eddy current damping and inherent friction. The dynamic characteristics of the TVMD, including inertial mass amplification and damping enhancement effects, were revealed.

2) Four parameter calibration methods were introduced: the peak point fitting method, hysteretic curve fitting method, time-history fitting method, and transfer function fitting method. While the transfer function fitting method offers an equivalent damping coefficient for tuning design, the remaining three methods can identify parameters for nonlinear damping models. The hysteretic curve fitting and time-history fitting methods provide superior accuracy in parameter identification compared with the other two methods, while the peak point fitting and transfer function fitting methods exhibit lower computational costs.

3) Three damping models were employed for parameter identification of the damping element of TVMD: the equivalent linear damping model, exponential damping model, and Wouterse damping model. The exponential damping model and Wouterse damping model exhibit superior fitting accuracy compared with the equivalent linear damping model. Particularly, the Wouterse damping model reflect the decrease in damping force at over-critical velocity.

References

[1] Lee D, Taylor D P. Viscous damper development and future trends[J]. *The Structural Design of Tall Buildings*, 2001, **10**(5): 311 − 320. DOI: 10.1002/tal.188.

[2] Miao Z W, Yang Y H, Cong R. Seismic performance improvement design for RC frame structures based on viscous dampers [J]. *Journal of Southeast University*, 2023, **53**(2): 210 − 217. DOI: 10.3969/j.issn.1001-0505.2023.02.004. (in Chinese)

[3] Gao H, Xing C X, Wang H, et al. Performance improvement of base-isolated structures by the tuned negative stiffness-inertial mass damper[J]. *Journal of Southeast University*, 2023, **53**(4): 592 − 599. DOI: 10.3969/j.issn.1001-0505.2023.04.004. (in Chinese)

[4] Kaynia A M, Veneziano D, Biggs J M. Seismic effectiveness of tuned mass dampers[J]. *Journal of the Structural Division*, 1981, **107**(8): 1465 − 1484. DOI: 10.1061/jsdeag.0005760.

[5] Ikago K, Saito K, Inoue N. Seismic control of single-degree-of-freedom structure using tuned viscous mass damper[J]. *Earthquake Engineering & Structural Dynamics*, 2012, **41**(3): 453 − 474. DOI: 10.1002/eqe.1138.

[6] Li Y F, Tan P, Li S Y, et al. A novel tuned inerter eddy current damper: Modeling, optimization, and evaluation [J]. *Engineering Structures*, 2023, **285**: 116026. DOI: 10.1016/j.engstruct.2023.116026.

[7] Li Y F, Tan P, Li S Y. Improving the control performance of optimal tuned inerter damper via nonlinear eddy current damping [J]. *Nonlinear Dynamics*, 2024, **112**(1): 331 − 352. DOI: 10.1007/s11071-023-09054-w.

[8] Zhang R F, Zhao Z P, Pan C, et al. Damping enhancement principle of inerter system[J]. *Structural Control and Health Monitoring*, 2020, **27**(5): e2523. DOI: 10.1002/stc.2523.
[9] Cheng Y H, Ji X D. Robustness of a tuned viscous mass damper (TVMD) controlled system[J]. *Advances in Structural Engineering*, 2022, **25**(16): 3349 - 3367. DOI: 10.1177/13694332221133209.
[10] Ji X D, Jia R F, Wang L J, et al. Seismic design and performance assessment of a retrofitted building with tuned viscous mass dampers (TVMD)[J]. *Engineering Structures*, 2024, **305**: 117688. DOI: 10.1016/j.engstruct.2024.117688.
[11] Ji X D, Zhang J S, Ikago K, et al. Tuned viscous mass damper (TVMD) coupled wall system for enhancing seismic performance of high-rise buildings[J]. *Engineering Structures*, 2021, **240**: 112307. DOI: 10.1016/j.engstruct.2021.112307.
[12] Sugimura Y, Goto W, Tanizawa H, et al. Response control effect of steel building structure using tuned viscous mass damper[C]//*Proceedings of the* 15*th World Conference on Earthquake Engineering*. Lisbon, Portugal, 2012, **9**: 24 - 28.
[13] Ji X D, Cheng Y H, Molina Hutt C. Seismic response of a tuned viscous mass damper (TVMD) coupled wall system[J]. *Engineering Structures*, 2020, **225**: 111252. DOI: 10.1016/j.engstruct.2020.111252.
[14] Jia R F, Ji X D, Cheng Y H, et al. Seismic response control of core wall structures using tuned viscous mass damper (TVMD) outriggers[J]. *Engineering Structures*, 2023, **292**: 116546. DOI: 10.1016/j.engstruct.2023.116546.
[15] Ogino M, Sumiyama T. Structural design of a high-rise building using tuned viscous mass dampers installed across three consecutive storeys[C]//*Proceedings of the Twelfth International Conference on Computational Structures Technology*. Naples, Italy, 2014: 225. DOI: 10.4203/ccp.106.225.
[16] Murakami K, Ishii M, Miyazaki K, et al. Proposal for an efficient damping system for high-rise buildings in major earthquakes[J]. *Journal of Disaster Research*, 2016, **11**(1): 106 - 117. DOI: 10.20965/jdr.2016.p0106.
[17] Smith M C. Synthesis of mechanical networks: The inerter[J]. *IEEE Transactions on Automatic Control*, 2002, **47**(10): 1648 - 1662. DOI: 10.1109/TAC.2002.803532.
[18] Wang F C, Hong M F, Lin T C. Designing and testing a hydraulic inerter[J]. *Proceedings of the Institution of Mechanical Engineers, Part C: Journal of Mechanical Engineering Science*, 2011, **225**(1): 66 - 72. DOI: 10.1243/09544062jmes2199.
[19] Swift S J, Smith M C, Glover A R, et al. Design and modelling of a fluid inerter[J]. *International Journal of Control*, 2013, **86**(11): 2035 - 2051. DOI: 10.1080/00207179.2013.842263.
[20] Liang R J, Wang H, Gao H, etc. Optimization of TMD for vibration reduction of wind turbine under seismic excitation[J]. *Journal of Southeast University*, 2021, **51**(2): 256 - 263. DOI: 10.3969/j.issn.1001-0505.2021.02.010. (in Chinese)
[21] Dai J, Xu Z D, Gai P P. Effects of frequency-dependence on viscoelastic tuned mass dampers[J]. *Journal of Southeast University*, 2018, **48**(2): 282 - 287. DOI: 10.3969/j.issn.1001-0505.2018.02.015. (in Chinese)
[22] Ikago K, Sugimura Y, Saito K, et al. Modal response characteristics of a seismic control multi-story shear building using a tuned viscous nass damper[C]//*Proceedings of the Fourteenth International Conference on Civil, Structural and Environmental Engineering Computing*. Cagliari, Sardinia, Italy, 2013: 41. DOI: 10.4203/ccp.102.41.
[23] Wouterse J H. Critical torque and speed of eddy current brake with widely separated soft iron poles[J]. *IEE Proceedings B: Electric Power Applications*, 1991, **138**(4): 153 - 158. DOI: 10.1049/ip-b.1991.0019.
[24] Cheng Y H, Ji X D, Ikago K, et al. Analytical solutions of H_2 control and efficiency-based design of structural systems equipped with a tuned viscous mass damper[J]. *Structural Control and Health Monitoring*, 2022, **29**(5): e2932. DOI: 10.1002/stc.2932.

调谐惯质阻尼器动力试验和参数识别

纪晓东　程禹皓　贾若凡　余　越

(清华大学土木工程安全与耐久教育部重点实验室, 北京 100084)

摘要:研发了一种新型调谐惯质阻尼器(TVMD)装置,该装置分别采用电涡流与金属弹簧作为 TVMD 的阻尼元件与弹簧元件. 首先,对该 TVMD 装置进行动力试验,研究其动力特性. 然后,提出 4 种基于试验数据识别 TVMD 参数的方法,即峰值点拟合法、滞回曲线拟合法、时程拟合法和传递函数拟合法. 动力试验结果表明:TVMD 具有惯性质量放大效应和阻尼增益效应;弹簧元件和惯容元件均表现出理想的线性特性,而阻尼元件由于电涡流阻尼固有属性和 TVMD 装置中存在的摩擦,表现出非线性特性. 参数识别结果表明:4 种方法均能合理确定 TVMD 参数,其中,传递函数拟合法能提供用于调谐设计的等效阻尼系数,而其他 3 种方法能识别非线性阻尼模型的参数;滞回曲线拟合法和时程拟合法具有更高的参数识别精度,而峰值点拟合法和传递函数拟合法具有更高的计算效率.

关键词:调谐惯质阻尼器(TVMD);动力试验;参数标定;阻尼非线性;振动控制

中图分类号:TU398.9